

# Geometric Nonlinear Analysis of Reinforced Concrete Folded Plate Structures by the Harmonic Coupled Finite Strip Method

Dragan D. Milašinović / Danica Goleš

Received 2013-04-23, revised 2013-11-04, accepted 2014-01-18

## Abstract

This paper presents theoretical and numerical analysis of two reinforced concrete folded plate structures (RCFPS) of span length 20 and 30 m, according to linear predictions and predictions of geometric nonlinear behavior of structure. Characteristic cross-sections are designed on the basics of internal forces calculated using linear finite strip method (FSM). The ultimate resistance of characteristic cross-sections is presented through diagrams of interaction. It was found that the safety factors of selected cross sections calculated assuming linear structural behavior in almost all the cases are on the safe side in relation to the results obtained assuming large displacements. Significant differences between the results of linear and nonlinear theory are observed only at longer RCFPS. The stability analysis required during the design process is performed by using the complex harmonic coupled finite strip method (HCFSM). A combined application of MPI and OpenMP parallelization methods in the cloud computing environment is used.

## Keywords

harmonic coupled finite strip method · reinforced concrete folded plate structures · ultimate resistance · cloud computing · MPI · OpenMP

## Dragan D. Milašinović

Faculty of Civil Engineering Subotica, University of Novi Sad, Kozaračka 2a, Subotica, Serbia  
e-mail: ddmil@gf.uns.ac.rs

## Danica Goleš

Faculty of Civil Engineering Subotica, University of Novi Sad, Kozaračka 2a, Subotica, Serbia  
e-mail: dgoles@gf.uns.ac.rs

## 1 Introduction

For very long time folded plate structures have been realized in practice only in reinforced concrete and made on site. Development of prefabricated building lead to improvements of this type of construction so that the folded structures could be derived by assembly of prefabricated elements and their connection-monolitization on site. Typical RCFPS taken into consideration here are simply supported by diaphragms and may have arbitrary longitudinal edge conditions.

There is a great deal of RCFPS for which both the geometry and the material properties can be considered as constants along a main direction, straight or curved, while, generally, only the loading distribution may vary (e.g. thin-walled beams, cylindrical and prismatic shell roofs [2] and box-girder bridges [3,4]). In many cases, the performance of these structures is also improved by means of proper longitudinal prestressing systems. For these structures, the design process should lead to define the optimal morphology of the transversal cross-section, which means its geometry, size, shape and topology, as well as the layout of the prestressing system, described by the prestressing forces and the cables profile.

In such context, the attention of this paper is focused on the optimal design of RCFPS composed by flat plates and subjected to multiple loading conditions, Fig. 1 (a). A proper modeling of these structures can be found within the framework of the FSM. As well known, this method is based on the formulation of a special class of finite elements that are as long as the structure and interconnected along the nodal lines that constitute the sides of the strips themselves. The FSM was originally developed by Cheung [1]. The well known uncoupled formulation, represents a semi-analytical finite element method (FEM). As far as linear analysis is concerned, it takes advantage of the orthogonality properties of harmonic functions in the stiffness matrix formulation.

However, in the case of the geometric nonlinear analysis, the integral expressions contain the products of trigonometric functions with higher-order exponents, and therefore the orthogonality characteristics are no longer valid. All harmonics are coupled, and the stiffness-matrix order and bandwidth are pro-

portional to the number of harmonics used. This kind of FSM analysis is named the HCFSM [5, 6].

Determination of elements of the strip stiffness matrices is very complex and represents the most time consuming part of the application execution. It requests calculation of a very large number of integral expressions for the large number of harmonics used (the number of integrals depends by power four to the number of used harmonics). Calculated integrals are necessary for the calculation of each strip stiffness matrix in the each iteration. Therefore, the integral expressions are calculated once, independent of particular strip length, and stored in a memory during the execution process [7]. Different optimization strategies for providing values of integrals have been described in [9, 12]. In order to cope with dramatic increase of computation time due to coupling of all series terms in HCFSM formulation, a combined application of MPI and OpenMP parallelization methods is used.

## 2 Harmonic coupled finite-strip stability equations

If a structure undergoes large displacements, the second order terms regarding the strains cannot be ignored. The strain-displacement relations, within the context of a Green-Lagrange strain tensor, represent a sum of linear and non-linear parts. Analysis of plates in the post-buckling range is generally performed on the basis of von Karman equations or by employing an energy approach. Only approximate solutions can be obtained, taking into account the in-plane (membrane) and out-of-plane (bending) boundary conditions.

The nonlinear strain-displacement relations in the FSM can be predicted by the combination of the plane elasticity and the Kirchhoff plate theory. Using this assumption in the Green-Lagrange strain tensor (Eq. (1)) for in-plane nonlinear strains gives Green-Lagrange HCFSM formulation. Also that, neglecting lower-order terms in a manner consistent with the usual von Karman assumptions gives HCFSM von Karman formulation.

$$\varepsilon_{ij} = 1/2 (u_{i,j} + u_{j,i} + u_{k,i}u_{k,j}) \quad (1)$$

In the FSM, which combines elements of the classical Ritz method and FEM, the general form of the displacement function  $f = \mathbf{A}\mathbf{q}$  can be written as a product of polynomials and trigonometric functions

$$f = \mathbf{A}\mathbf{q} = \sum_{m=1}^r \mathbf{A}_m \mathbf{q}_m = \sum_{m=1}^r y_m(y) \sum_{k=1}^c \mathbf{N}_k(x) \mathbf{q}_{km} \quad (2)$$

where  $Y_m(y)$  are functions from the Ritz method,  $\mathbf{N}_k(x)$  are interpolation functions from the FEM and  $r$  represents the total number of the series terms. The local Degrees Of Freedom (DOFs) are defined as the displacements and rotation of a nodal line (DOFs = 4), as shown in Fig. 1 (b). The DOFs are also called generalized coordinates.

If we introduce vectors

$$\mathbf{e}_0 = \begin{bmatrix} \frac{\partial u_0}{\partial x} \\ \frac{\partial v_0}{\partial y} \\ \frac{\partial u_0}{\partial y} + \frac{\partial v_0}{\partial x} \end{bmatrix}, \mathbf{e}'_0 = \begin{bmatrix} \frac{\partial u_0}{\partial x} \\ 0 \\ \frac{\partial u_0}{\partial y} \end{bmatrix}, \mathbf{e}''_0 = \begin{bmatrix} 0 \\ \frac{\partial v_0}{\partial y} \\ \frac{\partial v_0}{\partial x} \end{bmatrix},$$

$$\boldsymbol{\eta}_0 = \begin{bmatrix} 1/2 \left(\frac{\partial w}{\partial x}\right)^2 \\ 1/2 \left(\frac{\partial w}{\partial y}\right)^2 \\ \frac{\partial w}{\partial y} \frac{\partial w}{\partial x} \end{bmatrix}, \boldsymbol{\zeta}_0 = \begin{bmatrix} 1/2 \left(\frac{\partial u_0}{\partial x}\right)^2 \\ 1/2 \left(\frac{\partial u_0}{\partial y}\right)^2 \\ \frac{\partial u_0}{\partial y} \frac{\partial u_0}{\partial x} \end{bmatrix}, \boldsymbol{\chi} = \begin{bmatrix} -\frac{\partial^2 w}{\partial x^2} \\ -\frac{\partial^2 w}{\partial y^2} \\ -2\frac{\partial^2 w}{\partial x \partial y} \end{bmatrix}, \quad (3)$$

where  $u_0$ ,  $v_0$  and  $w = w_0$  are the displacement components of a point in the middle plane, the expressions for strains at an arbitrary point will now have the form

$$\boldsymbol{\varepsilon} = \boldsymbol{\varepsilon}_0 + z\boldsymbol{\chi},$$

$$\boldsymbol{\varepsilon}_0 = \mathbf{e}_0 + \boldsymbol{\eta}_0 + \boldsymbol{\zeta}_0 = \mathbf{e}'_0 + \mathbf{e}''_0 + \boldsymbol{\eta}_0 + \boldsymbol{\zeta}_0. \quad (4)$$

Once the displacement functions (Eq. (2)) are known, it is possible to obtain the strains as products of the following matrices and vectors

$$\mathbf{e}_0 = \mathbf{L}_1 \mathbf{A}_u \mathbf{q}_u, \quad \boldsymbol{\eta}_0 = 1/2 \mathbf{L}_1 \tilde{\mathbf{A}}_w \mathbf{W} \mathbf{L}_2 \mathbf{A}_w \mathbf{q}_w,$$

$$\boldsymbol{\zeta}_0 = 1/2 \mathbf{L}_1 \tilde{\mathbf{A}}_u^u \mathbf{U} \mathbf{L}_2 \mathbf{A}_u^u \mathbf{q}_u^u, \quad \boldsymbol{\chi} = \mathbf{L}_3 \mathbf{A}_w \mathbf{q}_w, \quad (5)$$

$$\mathbf{e}'_0 = \mathbf{L}_4 \mathbf{A}_u^u \mathbf{q}_u^u, \quad \mathbf{e}''_0 = \mathbf{L}_5 \mathbf{A}_w^v \mathbf{q}_w^v$$

where

$$\mathbf{L}_1 = \begin{bmatrix} \partial/\partial x & 0 \\ 0 & \partial/\partial y \\ \partial/\partial y & \partial/\partial x \end{bmatrix}, \mathbf{L}_2 = \begin{bmatrix} \partial/\partial x \\ \partial/\partial y \end{bmatrix},$$

$$\mathbf{L}_3 = \begin{bmatrix} -\partial^2/\partial x^2 \\ -\partial^2/\partial y^2 \\ -2\partial^2/\partial x \partial y \end{bmatrix}, \mathbf{L}_4 = \begin{bmatrix} \partial/\partial x \\ 0 \\ \partial/\partial y \end{bmatrix}, \mathbf{L}_5 = \begin{bmatrix} 0 \\ \partial/\partial y \\ \partial/\partial x \end{bmatrix}, \quad (6)$$

$$\mathbf{A}_u = \begin{bmatrix} \mathbf{A}_u^u & \mathbf{0} \\ \mathbf{0} & \mathbf{A}_u^v \end{bmatrix}, \mathbf{q}_u = \begin{bmatrix} \mathbf{q}_u^u \\ \mathbf{q}_u^v \end{bmatrix}, \tilde{\mathbf{A}}_w = \begin{bmatrix} \mathbf{A}_w & \mathbf{0} \\ \mathbf{0} & \mathbf{A}_w \end{bmatrix},$$

$$\mathbf{W} = \begin{bmatrix} \mathbf{q}_w & \mathbf{0} \\ \mathbf{0} & \mathbf{q}_w \end{bmatrix}, \tilde{\mathbf{A}}_u^u = \begin{bmatrix} \mathbf{A}_u^u & \mathbf{0} \\ \mathbf{0} & \mathbf{A}_u^u \end{bmatrix}, \mathbf{U} = \begin{bmatrix} \mathbf{q}_u^u & \mathbf{0} \\ \mathbf{0} & \mathbf{q}_u^u \end{bmatrix}.$$

$\mathbf{A}_u^u$ ,  $\mathbf{A}_u^v$  and  $\mathbf{A}_w$  are the corresponding approximative functions, while  $\mathbf{q}_u^u$ ,  $\mathbf{q}_u^v$  and  $\mathbf{q}_w$  represent the vectors of displacement parameters in the nodal lines.

Then we introduce the matrices, which are referred to as the strain matrices

$$\mathbf{B}_{u1} = \mathbf{L}_1 \mathbf{A}_u, \quad \mathbf{B}_{w1} = \mathbf{L}_1 \tilde{\mathbf{A}}_w, \quad \mathbf{B}_{w2} = \mathbf{L}_2 \mathbf{A}_w$$

$$\mathbf{B}_{u1}^u = \mathbf{L}_1 \tilde{\mathbf{A}}_u^u, \quad \mathbf{B}_{u2}^u = \mathbf{L}_2 \mathbf{A}_u^u, \quad \mathbf{B}_{w3} = \mathbf{L}_3 \mathbf{A}_w \quad (7)$$

$$\mathbf{B}_{u4}^u = \mathbf{L}_4 \mathbf{A}_u^u, \quad \mathbf{B}_{u5}^v = \mathbf{L}_5 \mathbf{A}_w^v,$$

The matrices  $\mathbf{B}_{u1} \dots \mathbf{B}_{u5}^v$  are obtained as first derivatives, and the matrix  $\mathbf{B}_{w3}$  as the second derivative of the corresponding displacement functions. Now we can write the strain vectors (Eq. (5)) in shorter form

$$\mathbf{e}_0 = \mathbf{B}_{u1} \mathbf{q}_u, \quad \boldsymbol{\eta}_0 = 1/2 \mathbf{B}_{w1} \mathbf{W} \mathbf{B}_{w2} \mathbf{q}_w, \quad \boldsymbol{\zeta}_0 = 1/2 \mathbf{B}_{u1}^u \mathbf{U} \mathbf{B}_{u2}^u \mathbf{q}_u^u,$$

$$\boldsymbol{\chi} = \mathbf{B}_{w3} \mathbf{q}_w, \quad \mathbf{e}'_0 = \mathbf{B}_{u4}^u \mathbf{q}_u^u, \quad \mathbf{e}''_0 = \mathbf{B}_{u5}^v \mathbf{q}_w^v \quad (8)$$

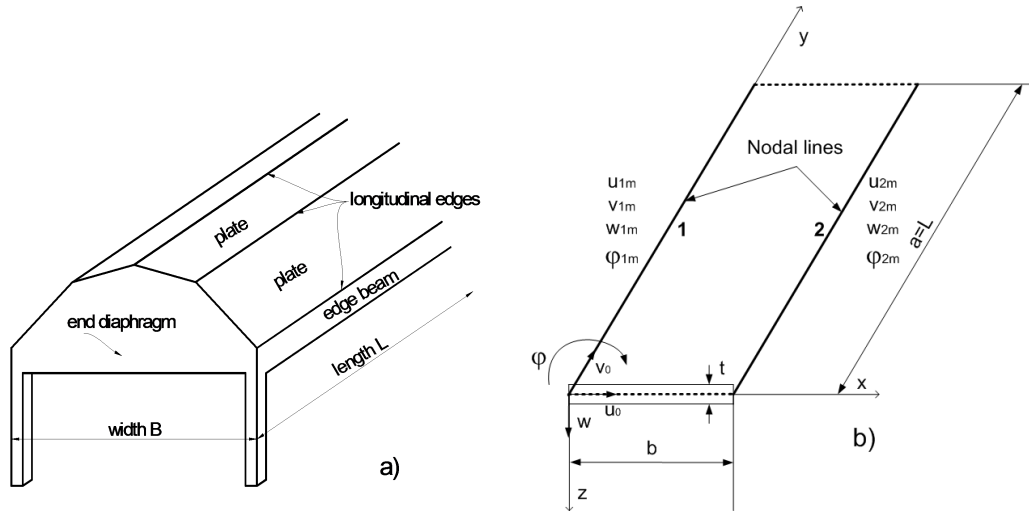


Fig. 1. (a) Elements of prismatic folded plate structure, (b) Simply supported flat shell strip

The strain energy of the strip is given by

$$U = 1/2 \int_V \boldsymbol{\varepsilon}^T \boldsymbol{\sigma} dV = \int_A \int_{-t/2}^{t/2} \left[ \boldsymbol{\varepsilon}_0^T \quad z\boldsymbol{\chi}^T \right] \begin{bmatrix} \mathbf{D} & \mathbf{D} \\ \mathbf{D} & \mathbf{D} \end{bmatrix} \begin{bmatrix} \boldsymbol{\varepsilon}_0 \\ z\boldsymbol{\chi} \end{bmatrix} dAdz$$

$$dAdz = 1/2 \int_A \boldsymbol{\varepsilon}_0^T \mathbf{D}_m \boldsymbol{\varepsilon}_0 dA + 1/2 \int_A \boldsymbol{\varepsilon}_0^T \mathbf{D}_{mb} \boldsymbol{\chi} dA + \int_A \boldsymbol{\chi}^T \mathbf{D}_b \boldsymbol{\chi} dA = U_m + U_{mb} + U_b \quad (9)$$

where  $U_m$  designates the membrane strain energy,  $U_{mb}$  the interaction between the membrane and bending actions, and  $U_b$  the bending strain energy.

For a homogeneous material, the following property matrices in the plane  $\mathbf{D}_m$  and the bending  $\mathbf{D}_b$  yield

$$\mathbf{D}_m = \int_{-t/2}^{t/2} \mathbf{D} dz, \quad \mathbf{D}_{mb} = \int_{-t/2}^{t/2} z \mathbf{D} dz = \mathbf{0}, \quad (10)$$

$$\mathbf{D}_b = \int_{-t/2}^{t/2} z^2 \mathbf{D} dz = (t^3/12) \mathbf{D}$$

The matrix  $\mathbf{D}$  is often referred to as the elasticity matrix. In the present formulation the more general case of orthotropic properties will be assumed in which the property matrix  $\mathbf{D}$  is

$$\mathbf{D} = \begin{bmatrix} E_x/(1-\mu_x\mu_y) & \mu_x E_y/(1-\mu_x\mu_y) & 0 \\ \mu_y E_x/(1-\mu_x\mu_y) & E_y/(1-\mu_x\mu_y) & 0 \\ 0 & 0 & G \end{bmatrix}, \quad (11)$$

$$\mu_x E_y/(1-\mu_x\mu_y) = \mu_y E_x/(1-\mu_x\mu_y)$$

The potential energy due to external surface loads  $\mathbf{p}$  can be written simply as

$$W = - \int_A \mathbf{f}^T \mathbf{p} dA \quad (12)$$

Substituting Eq. (2) into Eq. (12)

$$W = - \int_A \mathbf{q}^T \mathbf{A}^T \mathbf{p} dA \quad (13)$$

For a concentrated load, the above integral is reduced to the simple expression of load multiplied by corresponding displacement. For all other distributed loads the potential energy can be obtained through some simple integration process.

The total potential energy is the sum of the elastic strain energy stored in the strip and the potential energy of the loads. Thus

$$\begin{aligned} \Pi = U + W = (U_m + U_b) + W = & \left( 1/2 \int_A \mathbf{q}_u^T \mathbf{B}_{u1}^T \mathbf{D}_m \mathbf{B}_{u1} \mathbf{q}_u dA + \right. \\ & + 1/2 \int_A \mathbf{q}_w^T \mathbf{B}_{w3}^T \mathbf{D}_b \mathbf{B}_{w3} \mathbf{q}_w dA \left. \right) + \\ & + \left[ 1/8 \int_A \mathbf{q}_w^T \mathbf{B}_{w2}^T \mathbf{W}^T \mathbf{B}_{w1}^T \mathbf{D}_m \mathbf{B}_{w1} \mathbf{W} \mathbf{B}_{w2} \mathbf{q}_w dA + \right. \\ & + 1/4 \int_A \mathbf{q}_w^T \mathbf{B}_{w2}^T \mathbf{W}^T \mathbf{D}_m \mathbf{B}_{u1} \mathbf{q}_u dA + \\ & + 1/4 \int_A \mathbf{q}_u^T \mathbf{B}_{u1}^T \mathbf{D}_m \mathbf{B}_{w1} \mathbf{W} \mathbf{B}_{w2} \mathbf{q}_w dA \left. \right] \\ & + \left\{ 1/8 \int_A \mathbf{q}_u^T \mathbf{B}_{u2}^T \mathbf{U}^T \mathbf{B}_{u1}^T \mathbf{D}_m \mathbf{B}_{u1} \mathbf{U} \mathbf{B}_{u2} \mathbf{q}_u dA + \right. \\ & + 1/4 \int_A \mathbf{q}_u^T \mathbf{B}_{u4}^T \mathbf{D}_m \mathbf{B}_{u1} \mathbf{U} \mathbf{B}_{u2} \mathbf{q}_u dA + \\ & + 1/4 \int_A \mathbf{q}_u^T \mathbf{B}_{u2}^T \mathbf{U}^T \mathbf{B}_{u1}^T \mathbf{D}_m \mathbf{B}_{u4} \mathbf{q}_u dA + \\ & + 1/4 \int_A \mathbf{q}_u^T \mathbf{B}_{u5}^T \mathbf{D}_m \mathbf{B}_{u1} \mathbf{U} \mathbf{B}_{u2} \mathbf{q}_u dA + \\ & + 1/4 \int_A \mathbf{q}_u^T \mathbf{B}_{u2}^T \mathbf{U}^T \mathbf{B}_{u1}^T \mathbf{D}_m \mathbf{B}_{u5} \mathbf{q}_u dA + \\ & + 1/8 \int_A \mathbf{q}_w^T \mathbf{B}_{w2}^T \mathbf{W}^T \mathbf{B}_{w1}^T \mathbf{D}_m \mathbf{B}_{u1} \mathbf{U} \mathbf{B}_{u2} \mathbf{q}_u dA + \\ & + 1/8 \int_A \mathbf{q}_u^T \mathbf{B}_{u2}^T \mathbf{U}^T \mathbf{B}_{u1}^T \mathbf{D}_m \mathbf{B}_{w1} \mathbf{W} \mathbf{B}_{w2} \mathbf{q}_w dA \left. \right\} - \\ & - \int_A \mathbf{q}^T \mathbf{A}^T \mathbf{p} dA \quad (14) \end{aligned}$$

The multiplication results of the membrane and bending actions in the first bracket of Eq. (14) are uniquely defined and

uncoupled, whilst those in second [von Karman assumptions] and third bracket {Green-Lagrange approach} are functions of the displacements  $u_0$ ,  $v_0$  and  $w$ . Consequently, the membrane and bending actions are coupled in many ways.

In order to obtain the system of stability equations (SSE) from the variational relations, the principle of minimum total potential energy is invoked.

$$\begin{aligned} & (\hat{\mathbf{K}}_{uu}\mathbf{q}_u + \hat{\mathbf{K}}_{ww}\mathbf{q}_w) + [1/2 \tilde{\mathbf{K}}_{ww}\mathbf{q}_w + 1/2 \tilde{\mathbf{K}}_{wu}\mathbf{q}_u + 1/4 \tilde{\mathbf{K}}_{uw}\mathbf{q}_w] + \\ & + \{1/2 \tilde{\mathbf{K}}_{uu}^{uu}\mathbf{q}_u^u + 3/4 \tilde{\mathbf{K}}_{uu}^{uu*}\mathbf{q}_u^u + 3/4 \tilde{\mathbf{K}}_{uu}^{uu**}\mathbf{q}_u^u + 1/4 \tilde{\mathbf{K}}_{uu}^{vu}\mathbf{q}_u^u + \\ & + 1/2 \tilde{\mathbf{K}}_{uu}^{uv}\mathbf{q}_u^v + 1/4 \tilde{\mathbf{K}}_{wu}^u\mathbf{q}_u^u + 1/4 \tilde{\mathbf{K}}_{uw}^u\mathbf{q}_w\} - \mathbf{Q} = \mathbf{0} \end{aligned} \quad (15)$$

The basic and the geometric stiffness matrices are, respectively

$$\begin{aligned} & \left( \hat{\mathbf{K}}_{uu} = \int_A \mathbf{B}_{u1}^T \mathbf{D}_m \mathbf{B}_{u1} dA, \quad \hat{\mathbf{K}}_{ww} = \int_A \mathbf{B}_{w3}^T \mathbf{D}_b \mathbf{B}_{w3} dA \right) \\ & \left[ \tilde{\mathbf{K}}_{ww} = \int_A \mathbf{B}_{w2}^T \mathbf{W}^T \mathbf{G}_1 \mathbf{W} \mathbf{B}_{w2} dA, \quad \tilde{\mathbf{K}}_{wu} = \int_A \mathbf{B}_{w2}^T \mathbf{W}^T \mathbf{G}_2 dA, \right. \\ & \left. \tilde{\mathbf{K}}_{uw} = \int_A \mathbf{G}_2^T \mathbf{W} \mathbf{B}_{w2} dA, \right] \left\{ \tilde{\mathbf{K}}_{uu}^{uu} = \int_A \mathbf{B}_{u2}^{uT} \mathbf{U}^T \mathbf{G}_3 \mathbf{U} \mathbf{B}_{u2}^u dA, \right. \\ & \tilde{\mathbf{K}}_{uu}^{uu*} = \int_A \mathbf{G}_4 \mathbf{U} \mathbf{B}_{u2}^u dA, \quad \tilde{\mathbf{K}}_{uu}^{uu**} = \int_A \mathbf{B}_{u2}^{uT} \mathbf{U}^T \mathbf{G}_4^T dA, \\ & \tilde{\mathbf{K}}_{uu}^{vu} = \int_A \mathbf{G}_5 \mathbf{U} \mathbf{B}_{u2}^u dA, \quad \tilde{\mathbf{K}}_{uu}^{uv} = \int_A \mathbf{B}_{u2}^{uT} \mathbf{U}^T \mathbf{G}_5^T dA, \\ & \left. \tilde{\mathbf{K}}_{wu}^u = \int_A \mathbf{B}_{w2}^T \mathbf{W}^T \mathbf{G}_6 \mathbf{U} \mathbf{B}_{u2}^u dA, \quad \tilde{\mathbf{K}}_{uw}^u = \int_A \mathbf{B}_{u2}^{uT} \mathbf{U}^T \mathbf{G}_6^T \mathbf{W} \mathbf{B}_{w2} dA \right\} \end{aligned} \quad (16)$$

where

$$\begin{aligned} & \left[ \mathbf{G}_1 = \mathbf{B}_{w1}^T \mathbf{D}_m \mathbf{B}_{w1}, \quad \mathbf{G}_2 = \mathbf{B}_{w1}^T \mathbf{D}_m \mathbf{B}_{u1}, \right] \\ & \left\{ \mathbf{G}_3 = \mathbf{B}_{u1}^{uT} \mathbf{D}_m \mathbf{B}_{u1}^u, \quad \mathbf{G}_4 = \mathbf{B}_{u4}^{uT} \mathbf{D}_m \mathbf{B}_{u1}^u, \right. \\ & \left. \mathbf{G}_5 = \mathbf{B}_{u5}^{vT} \mathbf{D}_m \mathbf{B}_{u1}^u, \quad \mathbf{G}_6 = \mathbf{B}_{w1}^T \mathbf{D}_m \mathbf{B}_{u1}^u \right\} \end{aligned} \quad (17)$$

We can visualize the construction of a strip stiffness matrix, which is composed of twelve block matrices. Assembling block matrices into conventional/geometric stiffness matrix of each strip is performed according to the scheme presented in Fig. 2, where:  $ST1 = \hat{\mathbf{K}}_{uu}$ ,  $ST2 = \hat{\mathbf{K}}_{ww}$ ,  $ST3 = \tilde{\mathbf{K}}_{ww}$ ,  $ST4 = \tilde{\mathbf{K}}_{wu}$ ,  $ST5 = \tilde{\mathbf{K}}_{uw}$ ,  $ST6 = \tilde{\mathbf{K}}_{uu}^{uu}$ ,  $ST7 = \tilde{\mathbf{K}}_{uu}^{uu*}$ ,  $ST8 = \tilde{\mathbf{K}}_{uu}^{uu**}$ ,  $ST9 = \tilde{\mathbf{K}}_{uu}^{vu}$ ,  $ST10 = \tilde{\mathbf{K}}_{uw}^u$ ,  $ST11 = \tilde{\mathbf{K}}_{wu}^u$  and  $ST12 = \tilde{\mathbf{K}}_{uw}^u$  ( $ST5 = ST4^T$ ,  $ST8 = ST7^T$ ,  $ST10 = ST9^T$ ,  $ST12 = ST11^T$ ).

### 3 Finite-Strip Program Visualization and Parallelization

The HCFSM software for geometric nonlinear analysis of thin plate structures requires long numerical computations and generates huge amount of numerical data, see Ref. [7, 9] and [12]. In this paper only short overview of the finite-strip program visualization and parallelization is presented.

To cope with such huge number of data, it is necessary to use suitable data visualization. These data constitute of incremental displacements and internal forces. They are produced

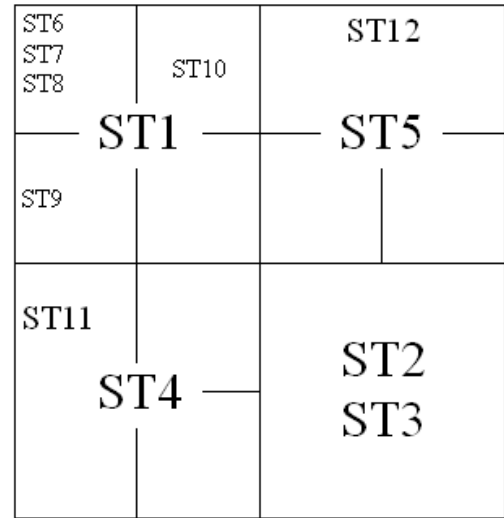


Fig. 2. Strip stiffness matrix assembling

in human readable format by different HCFSM implementations (each programmed in different programming languages: FORTRAN, C, C++), and ought to be translated from human readable format into special visualization format. Such formatted data serve as an input for special data visualization module which offers different graphical representations of the numerical results thus greatly simplifying the analyze process. They are shown in figures of the chapter 4.

The main part of the HCFSM application is an implementation of iterative numerical procedure for calculation of large displacements and inner forces of thin plate structures under multiple loading conditions. Based on the input data describing structure under consideration iterative process is started with the aim of finding displacement solutions which will meet previously set criteria. During the each iteration step, stiffness matrices and load vectors are generated for each strip and assembled into system stiffness matrix and system load vector later used for solving the SSE.

A very large number of integrals, calculated for the large number of harmonics used, are included for the calculation of each strip stiffness matrix in the each iteration. Some optimization strategies for providing values of integrals have been described in [9, 12]. In this research, integral expressions are calculated once, independent of particular strip length, and stored in a memory during the execution process. This approach represents the parallel HCFSM algorithm which combines the MPI/OpenMP [8, 13] programming models.

Parallelization effort in this research directly tackles the most computationally expensive part of the program. Profiling of HCFSM program execution, when the Green-Lagrange formulation is applied, suggests that the most time consuming part is computation of the stiffness matrices for every strip, whereas much less time is spent on finding the solution to SSE using the method of Gaussian elimination [9].

Calculations of stiffness matrix for different strips are independent and can be carried out in parallel on different proces-

sors. Therefore it is natural to use parallel programming libraries, such as MPI to obtain parallel calculation of stiffness matrix for different strips. Such approach allows substantial speedup as calculation of each stiffness matrix requires huge number of arithmetic operations to be conducted on relatively small set of input data. The cost-effective way to achieve the speedup is to use cluster composed of suitable number of nodes.

The usual MPI approach to parallel programming uses one node (called master node) to coordinate other nodes (called slave nodes) to execute specific tasks. Data are distributed evenly among the nodes and perfect load balancing is achieved in cases when all nodes are in charge of the same number of strips. One limitation of this approach is that the maximum number of nodes that can be processed in a particular computation depends on the number of strips in the problem. This means that for inputs with only a few strips, only a few computational nodes can be used. However, this limitation is not significant because inputs with a small number of strips are usually computationally light, and therefore great computing power is not really needed.

The second parallelization level deals with simultaneous computation of the block matrices (Fig. 2). The block matrices that depend solely on the geometrical properties of the strip, namely  $ST_1$  and  $ST_2$ , are computed only once and used as a basis for construction of the stiffness matrices. The remaining 10 block matrices are recomputed in each iteration based on the values of displacements for all harmonics. However, not all of them are of equal computational intensity. The four block stiffness matrices, namely  $ST_3$ ,  $ST_{11}$ ,  $ST_{12}$ , and  $ST_6$  (in decreasing order of their contributions), amount to 94% of the time needed for computing the stiffness matrices of all strips, and offer opportunity to apply parallel programming within one SMP node taking advantage of the globally shared address space. We refer to it as OpenMP approach. OpenMP is an industry standard for shared memory parallel programming. It is based on a fork-and-join execution model whereby the master thread forks a specified number of slave threads which execute blocks of code in parallel. By the end of the parallel region all threads had reached the barrier and only the master thread continues execution of user code beyond the end of the parallel construct. The advantage of OpenMP is that an existing code can be easily parallelized by placing OpenMP directives to denote parallel task sections which do not contain data dependencies, leaving the source code unchanged.

The hybrid approach, consisting of the two-level parallelization combining two different parallelization methods, gives good results, as cumulative speedup is almost 5 times.

#### 4 Numerical examples

Two RCFPSs of span length  $L = 20$  m and  $L = 30$  m, whose characteristic cross-section, applied service load and finite strip mesh are shown in Fig. 3, were analyzed. Structures are made of concrete C35/45 and reinforcement B400.

Maximum applied load is adopted as the triple value of the service load shown in Fig. 3, in order to reach the limit state

of structure. This maximum load is divided into a total of 37 increments. The symmetry of geometry, loads and supporting conditions is utilized, so the numerical analysis is carried out for only half of the structure. Young's elasticity modulus for concrete  $E = 34000$  MPa and zero Poisson's ratio are taken in the computations. Comparative analysis is done for linear (LIN), von Karman (VK) and Green-Lagrange (LAG) predictions.

The corresponding load in term of the tangent stiffness matrix (TSM) eigenvalue  $\lambda$  is depicted in Fig. 4. It can be concluded that all equilibrium states are stable because all  $\lambda_i > 0$ . However, as results of geometrical nonlinearity, the diagrams are quite different to shorter (hardening) and longer (softening) structures.

The differences between the transient cross-section deformation configurations, which are plotted in Fig. 5, show the influence of the length and load intensity to shorter and longer structures.

Fig. 6 shows the results obtained for central displacements  $w$  for shorter and longer structures. The straight lines represent the corresponding linear solutions.

Load to membrane forces ( $N_x$  and  $N_y$ ) and bending moment  $M_x$  curves are shown in Fig. 7 and Fig. 8.

Fig. 9 illustrates the convergence of the central displacements  $w$  for the last loading level. The convergence is nonmonotonic and fast.

Fig. 10 shows the convergence behavior of the membrane force  $N_x$  and the bending moment  $M_x$  with 21 harmonics used in the computations. The convergence is nonmonotonic and poor.

In Fig. 11, the distributions of the membrane force  $N_y$  ( $\Sigma m = 1 \dots 21$ ) along the transverse cross-section at midspan are shown at three loading levels. The effect of nonlinear behavior is more prominent in the Green-Lagrange prediction.

Comparative analysis of nonlinear effects between von Karman and Green-Lagrange approaches for both short and long structure is presented in Fig. 12.

Limit state design of characteristic cross sections is performed according to EC 2, on the basis of internal forces calculated by linear FSM. Diagrams of interaction ( $N_u - M_u$ ) of two characteristic cross sections of both RCFPSs are drawn using working diagrams (WD) of concrete and steel according to EC 2 (line A) and according to rheological-dynamical analogy (RDA) with maximum strain in concrete limited to  $\varepsilon_{cu} = 3.5\%$  (line B, see Ref. [6]) – Fig. 13 to Fig. 16. Partial safety factors for material are not applied. Tension force is treated as negative. Positive bending moment of the border beam stretches the bottom side of cross-section.

By comparing the behavior of normal force-bending moment ( $N - M$ ) function when increasing the load on diagrams of interaction shown in Fig. 13 to Fig. 16, i.e. magnified in Fig. 17, it is noted that the nonlinear behavior is much more pronounced in the longer structure. The influence of large displacements is particularly pronounced in the border beam according to LAG prediction.  $N - M$  path drawn by VK prediction in all analyzed cases is very close to linear behavior.

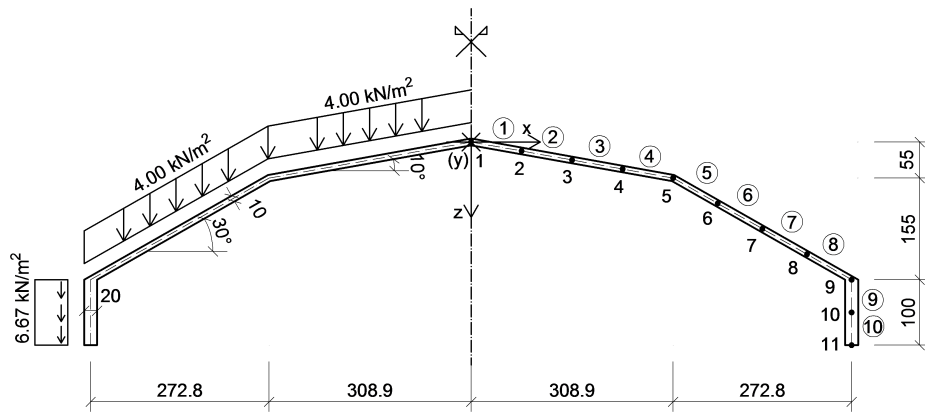


Fig. 3. RCFPSs cross-section, service load and strip idealization

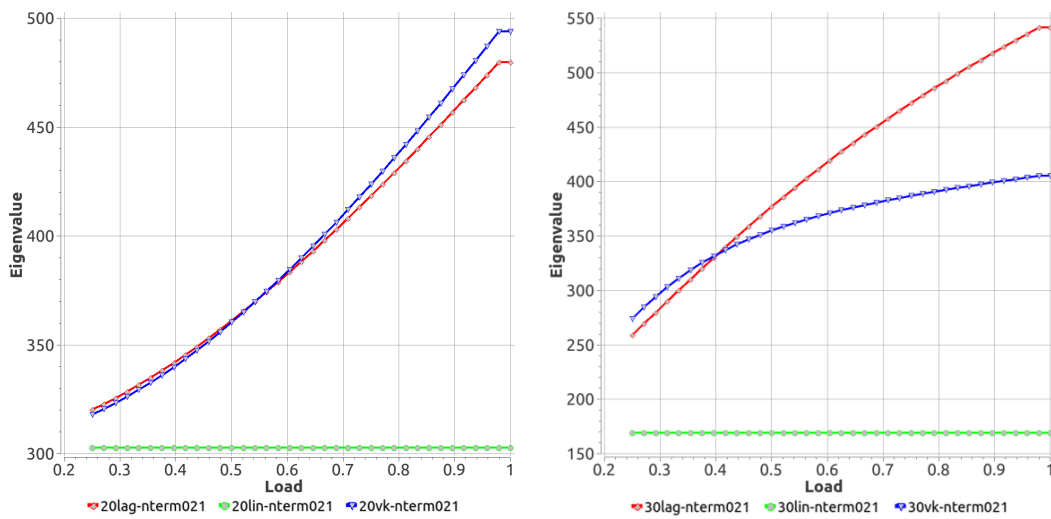


Fig. 4. Variation of TSM eigenvalue with load intensity for 21 series terms:  $L=20$  m (left) and  $L=30$  m (right)

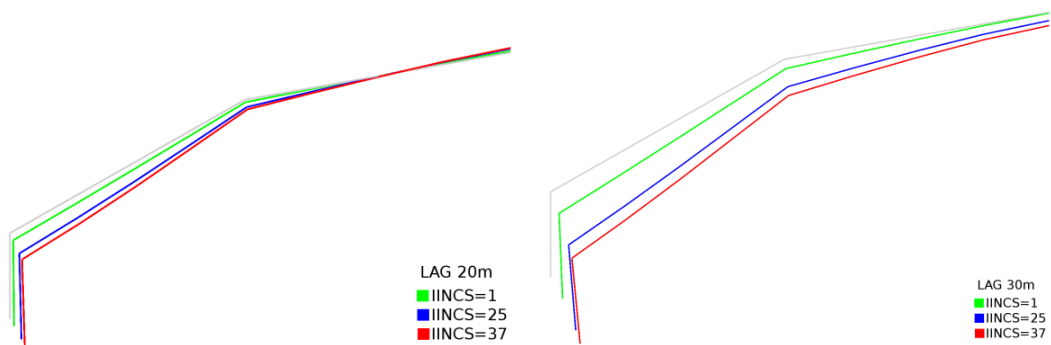


Fig. 5. The transient cross-section deformation configurations along the transverse cross-section at midspan:  $L=20$  m (left) and  $L=30$  m (right)

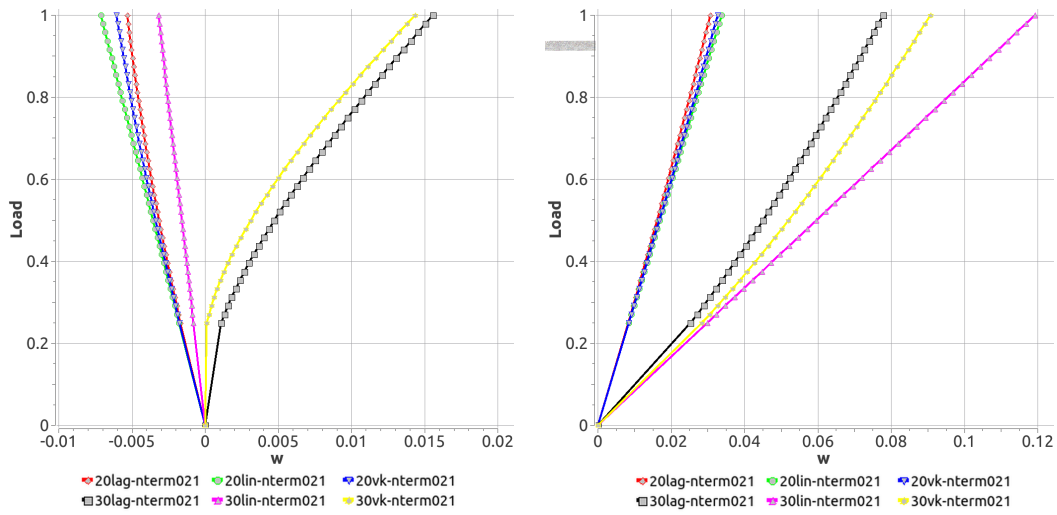


Fig. 6. Central displacement  $w$ : nodal line 1 (left) and nodal line 11 (right)

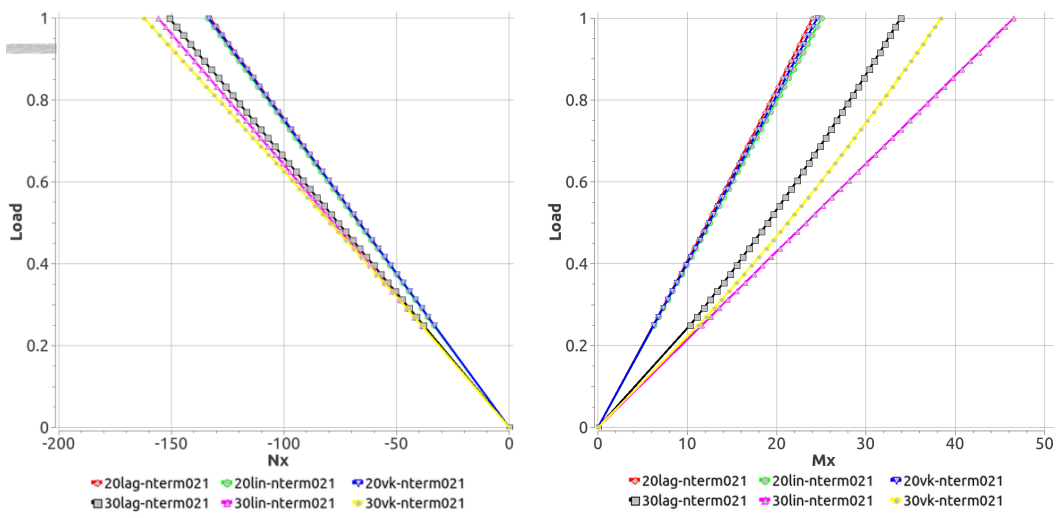


Fig. 7. Central membrane force  $N_x$  and central bending moment  $M_x$  (nodal line 1)

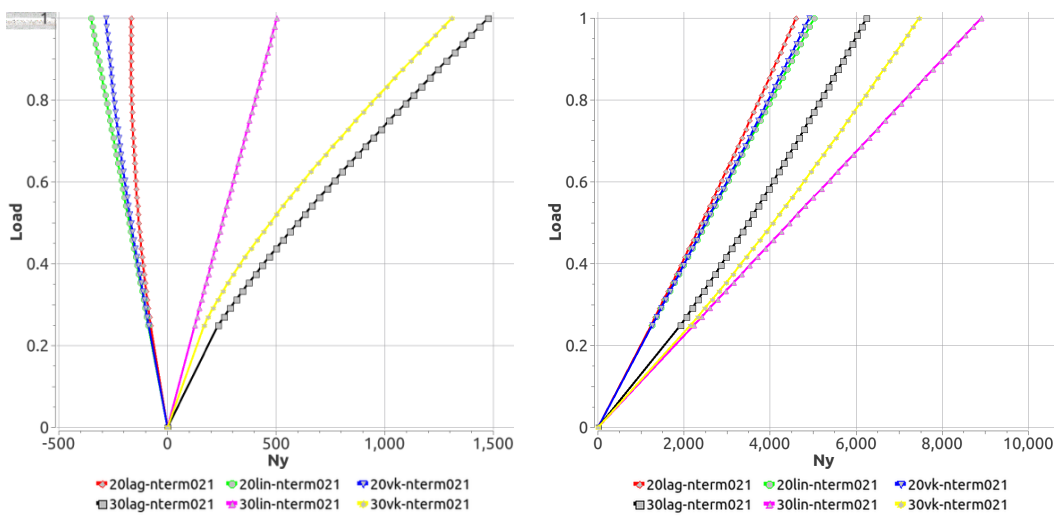


Fig. 8. Central membrane forces  $N_y$  in nodal line 9 (left) and nodal line 11 (right)

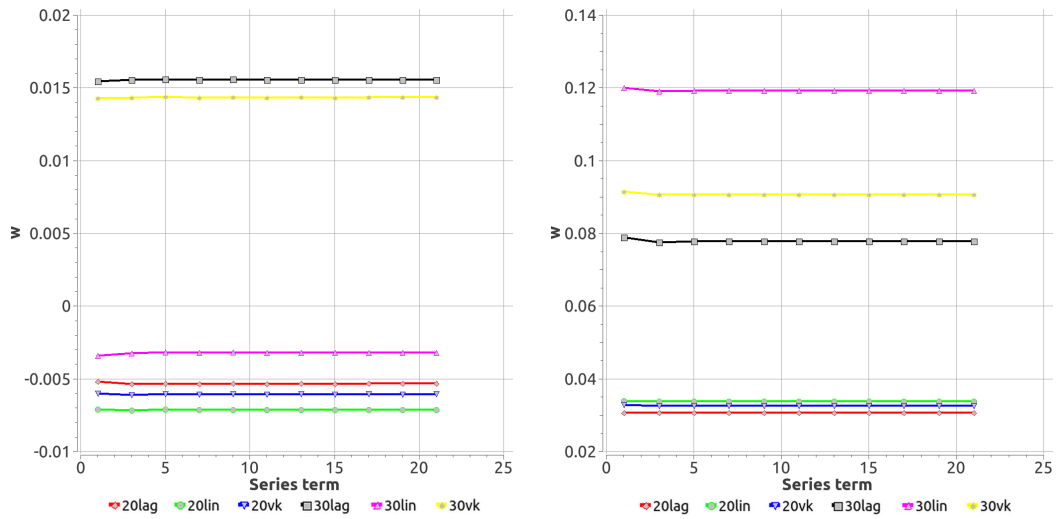


Fig. 9. HCFSM convergence of the central displacement  $w$ : nodal line 1 (left) and nodal line 11 (right)

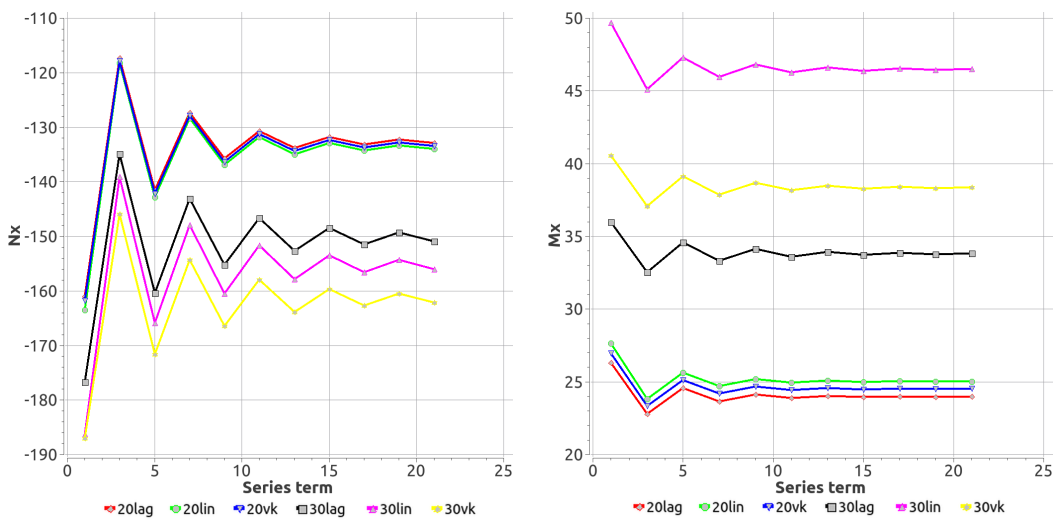


Fig. 10. HCFSM convergence of the central membrane force  $N_x$  and the central bending moment  $M_x$  (nodal line 1)

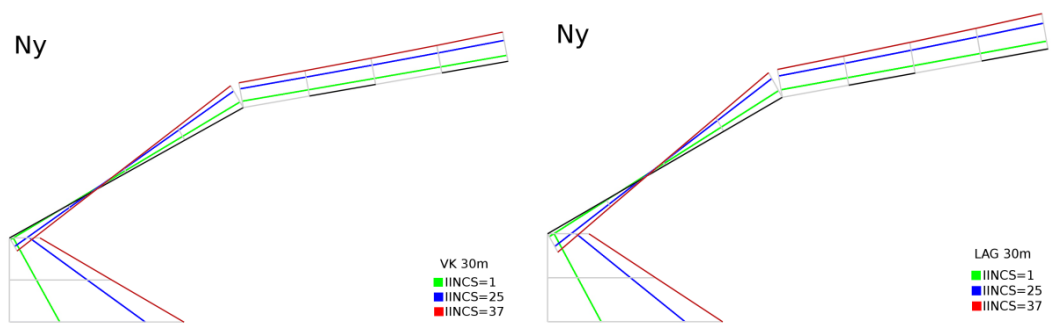


Fig. 11. Membrane forces along the transverse cross-section at midspan ( $L = 30\text{m}$ ): von Karman (left) and Green-Lagrange approach (right)

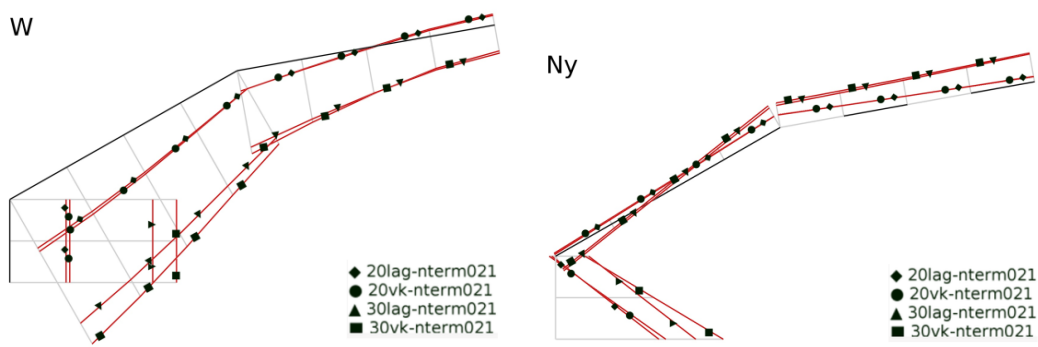


Fig. 12. Comparative analysis of nonlinear effects between von Karman and Green-Lagrange predictions

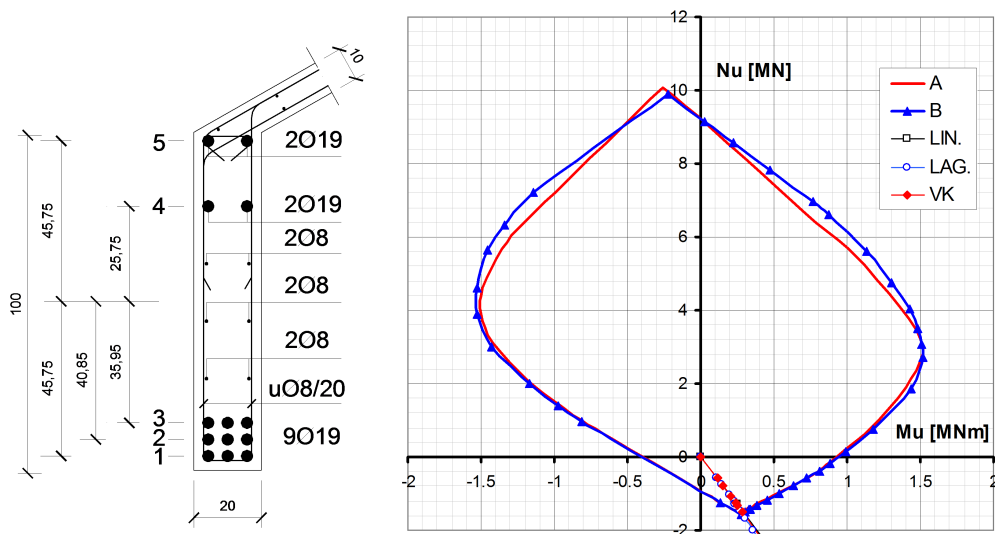


Fig. 13. RCFPS of  $L = 20$  m - Cross-section of the border beam at midspan and corresponding  $N_u - M_u$  diagram

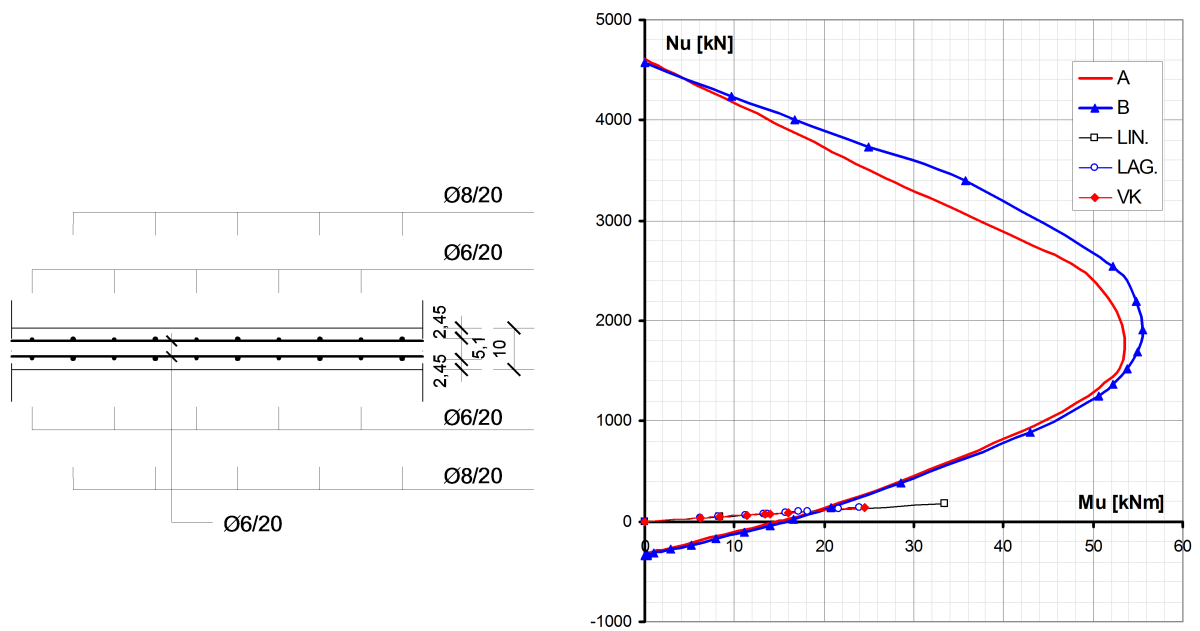


Fig. 14. RCFPS of  $L = 20$  m: Cross-section in nodal line 1 and corresponding  $N_u - M_u$  diagram

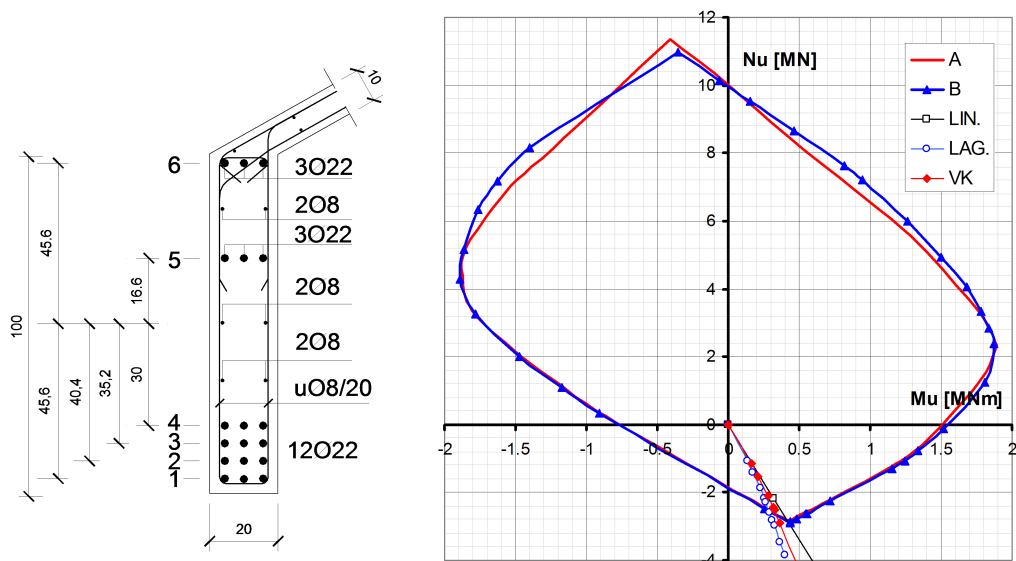


Fig. 15. RCFPS of  $L = 30$  m - Cross-section of the border beam at midspan and corresponding  $N_u - M_u$  diagram

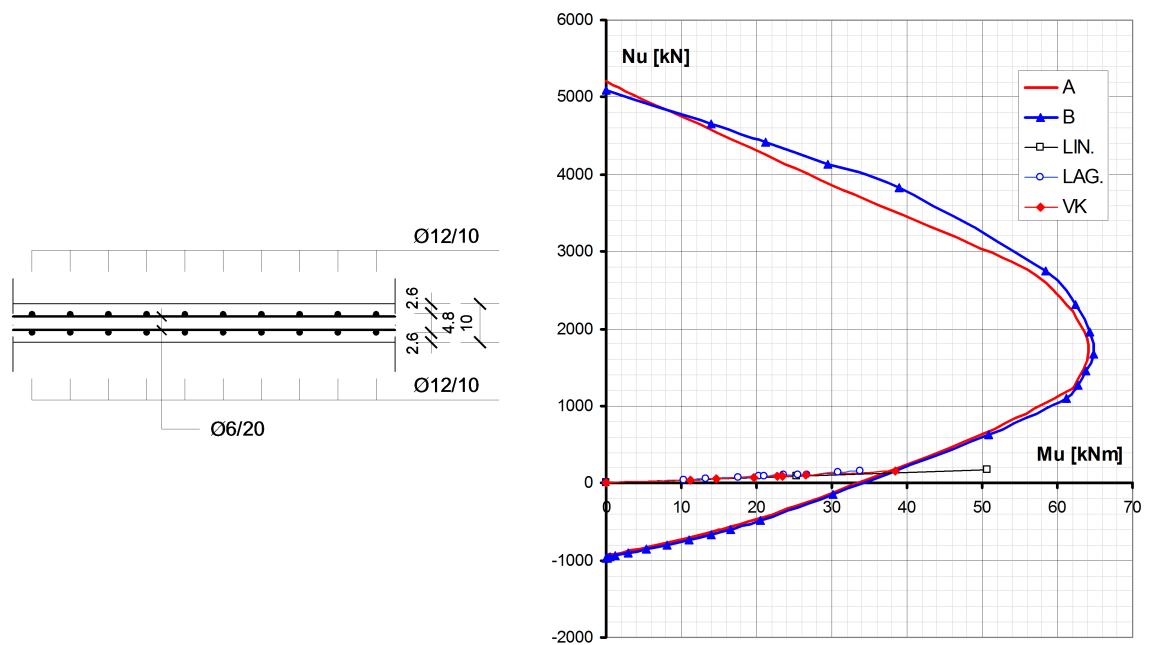
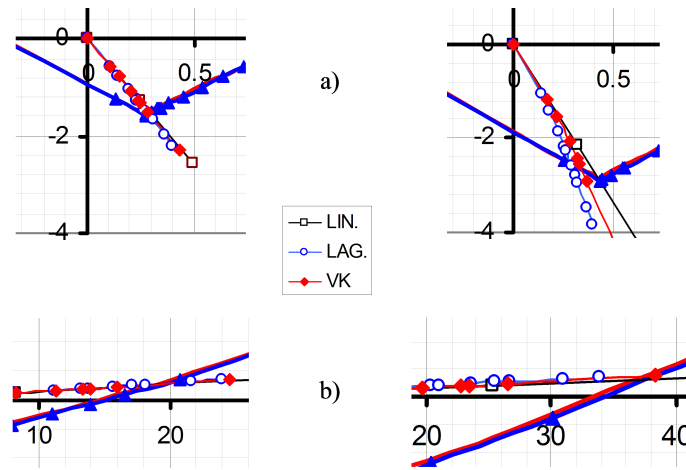


Fig. 16. RCFPS of  $L = 30$  m: Cross-section in nodal line 1 and corresponding  $N_u - M_u$  diagram



**Fig. 17.** Behavior of  $N - M$  function with load increase according to linear (LIN), Green-Lagrange (LAN) and von Karman (VK) predictions: (a) in border

beam and (b) in nodal line 1, for RCFPSs of span length  $L = 20\text{m}$  (left) and  $L = 30\text{m}$  (right)

The ultimate resistance ( $N_u$ ) and global safety factors  $\gamma(N) = N_u/N$  and  $\gamma(q) = q_u/q$  of two selected cross-sections of both RCFPSs, according to LIN, LAG and VK predictions are shown in Table 1 and Table 2. Here  $N$  and  $q$  are the membrane force due to service load and service load, respectively; the ultimate resistance  $N_u$  is taken from diagram of interaction at intersection of curve that represents the behavior of  $N - M$  function with load increase and the curve of fracture  $N_u - M_u$ , while  $q_u$  is the ultimate load at which the ultimate resistance  $N_u$  of the cross-section is reached.

From Table 1 and Table 2 it can be seen that the global safety factors of the cross sections, obtained by LIN predictions, almost always are on the safety side, or very close to the values from the LAG and VK predictions. The only exception are the safety factors in the border beam of longer RCFPS, where VK prediction gives  $\gamma(N)$  for 4.6% (for the curve A) and 4.4% (for the curve B) lower than the corresponding safety factors calculated by LIN prediction, while the safety factors  $\gamma(q)$  differ from the same for 2.4% and 2.2%. It is interesting that at the same time VK gives ultimate normal force ( $N_u$ ) 6% lower than predicted by LIN.

In the analyzed cross section of the border beam global safety factors are almost identical regardless of whether the linear or nonlinear predictions are applied, irrespective of the span length. However, the influence of the RCFPS's span length on its behavior is clearly visible in nodal line 1 at midspan. While at RCFPS of span length  $L = 20\text{m}$  safety factors are almost identical for all predictions, at longer RCFPS safety factor  $\gamma(N)$  by VK prediction is 30% higher than according to LIN prediction, and the corresponding  $\gamma(q)$  is higher by 25.91%. This again confirms that the linear theory gives the lower values of ultimate resistance of cross section than the nonlinear theory, i.e. that the results of linear analysis are in most cases on the safe side. As can be seen from Fig. 17 (b) the right, according to LAG prediction the ultimate bearing capacity of the cross section in nodal line 1 at midspan of longer structure is not reached even at max-

imum load analyzed, and in this case the value of safety factors in Table 2 could not be calculated.

Safety factors for non-linear predictions in relation to the service load  $\gamma(q)$  are different from the safety factors determined in relation to the membrane force due to service load  $\gamma(N)$  and in most of the analyzed cross sections is  $\gamma(q) > \gamma(N)$ . In most analyzed cases the ultimate limit state by nonlinear predictions is reached at higher load levels than in the case of linear behavior.

## 5 Conclusions

Adoption of the optimal RCFPS's design method depends on the desired accuracy on one and the complexity (cost) of analysis on the other side. Therefore, in this paper the numerical analysis of two RCFPS of span length 20 and 30 m is performed, using a simpler method - linear FSM and much more complex and demanding nonlinear methods (LAG and VK).

Based on comparative analysis of the results obtained by linear and nonlinear predictions it is observed that in RCFPS of span length 20 m such results are very similar. This means that the linear FSM is optimal method for the design of shorter RCFPSs. However, in RCFPS of span length 30 m difference between global safety factors of analysed cross sections according to linear and nonlinear predictions is up to 30%. Results obtained by linear FSM are almost always on the safe side in relation to the nonlinear predictions. Thus, by nonlinear analysis methods material savings can be achieved, but at the cost of increase in the price of analysis procedure.

The finite strip analysis of geometric nonlinear folded-plate structures is performed applying the von Karman and Green-Lagrange predictions for strains, which are both characterized by the coupling of all harmonics. The coupling of all series terms dramatically increases calculation time in an existing finite-strip sequential program when a large number of series terms are used.

The HCFSM algorithm offers good potential for both MPI and OpenMP parallelization. Therefore it is not surprise that

**Tab. 1.** The ultimate resistance and global safety factors of the cross-section in nodal line 1 at midspan

Span length		L = 20 m		L = 30 m	
Combination of working diagrams of concrete and steel		A	B	A	B
linear (LIN)	effects of service load	N = -777.75kN; M = 149.62 kNm		N = -1556.753 kN; M = 230.19 kNm	
	$N_u$	-1490	-1520	-2830	-2870
	$\gamma(N)$	1.916	1.954	1.818	1.843
	$\gamma(q)$	1.916	1.954	1.818	1.843
Green-Lagrange (LAG)	effects of service load	N = -763.477 kN; M = 143.912 kNm		N = -1401.483 kN; M = 176.17 kNm	
	$N_u$	-1505	-1550	-2540	-2560
	$\gamma(N)$	1.971	2.03	1.812	1.827
	$\gamma(q)$	2.008	2.07	1.905	1.922
von Karman (VK)	effects of service load	N = -776.517kN; M = 148.951kNm		N = -1533.584kN; M = 213.33kNm	
	$N_u$	-1490	-1520	-2660	-2700
	$\gamma(N)$	1.919	1.957	1.734	1.761
	$\gamma(q)$	1.926	1.965	1.7745	1.8025

**Tab. 2.** The ultimate resistance and global safety factors of the cross-section in nodal line 1 at midspan

Span length		L = 20 m		L = 30 m	
Combination of working diagrams of concrete and steel		A	B	A	B
linear (LIN)	effects of service load	N = 44.568 kN; M = 8.35 kNm		N = 51.647 kN; M = 15.339 kNm	
	$N_u$	99	105	120	128
	$\gamma(N)$	2.221	2.356	2.323	2.478
	$\gamma(q)$	2.221	2.356	2.323	2.478
Green-Lagrange (LAG)	effects of service load	N = 44.325 kN; M = 8.22 kNm		N = 50.741 kN; M = 13.32 kNm	
	$N_u$	100	105	not reached	not reached
	$\gamma(N)$	2.256	2.369	-	-
	$\gamma(q)$	2.260	2.373	-	-
von Karman (VK)	effects of service load	N = 44.335 kN; M = 8.30 kNm		N = 52.309 kN; M = 14.70 kNm	
	$N_u$	100	105	158	170
	$\gamma(N)$	2.256	2.368	3.02	3.25
	$\gamma(q)$	2.254	2.365	2.925	3.143

MPI/OpenMP hybrid approach shows good results in the parallelisation. In this paper only short overview of the finite-strip program visualization and parallelization is presented.

### Acknowledgements

The work reported in this paper is a part of the investigation within the research projects: ON 174027 “Computational Mechanics in Structural Engineering” and TR 36017 “Utilization of by-products and recycled waste materials in concrete composites in the scope of sustainable construction development in Serbia: investigation and environmental assessment of possible applications”, supported by the Ministry for Science and Technology, Republic of Serbia. This support is gratefully acknowledged.

### References

- 1 **Cheung YK**, *Finite Strip Method*, CRC Press LLC, 1998.
- 2 *Design of Cylindrical Concrete Shell Roofs, Manual of Engineering Practice*, ASCE; New York, USA, 1952.
- 3 **Kristek V**, *Theory of Box Girder Bridges*, John Wiley and Sons; Prague, Czech Republic, 1979.
- 4 **Loo YC, Cusens AR**, *The Finite Strip Method in Bridge Engineering*, E. & F. N. Spon; London, United Kingdom, 1978.
- 5 **Milašinović DD**, *Geometric non-linear analysis of thin plate structures using the harmonic coupled finite strip method*, *Thin-Walled Structures*, **49**(2), (2011), 280–290, DOI 10.1016/j.tws.2010.11.005.
- 6 **Milašinović DD, Goleš D, Borković A, Kukaras D, Landović A, Živanov Ž, Rakić P**, *Rheological-Dynamical Limit Analysis of Reinforced Concrete Folded Plate Structures using the Harmonic Coupled Finite-Strip Method*, In: **Topping BHV** (ed.), *Proceedings of the Eleventh International Conference on Computational Structures Technology*, Civil-Comp Press; Stirlingshire, UK, 2012, DOI 10.4203/ccp.99.158, paper 158.
- 7 **Milašinović DD**, *The Finite Strip Method in Computational Mechanics*, Faculties of Civil Engineering: University of Novi Sad, Technical University of Budapest and University of Belgrade; Subotica, Budapest, Belgrade, 1997.
- 8 *MPI: A Message-Passing Interface Standard, Version 2.2. MPI Forum (2009)*, <http://www.mpi-forum.org/docs/mpi-2.2/mpi22-report.pdf>.
- 9 **Nikolić M, Milašinović DD, Živanov Ž, Mari P, Hajduković M, Borković A, Milaković I**, *MPI/OpenMP Parallelisation of the Harmonic Coupled Finite-Strip Method*, In: **Iványi P, Topping BHV** (eds.), *Proceedings of the Second International Conference on Parallel, Distributed, Grid and Cloud Computing for Engineering*, Civil-Comp Press; Stirlingshire, UK, 2011, DOI 10.4203/ccp.95.94, paper 94.
- 10 *OpenMP, Wikipedia article*, <http://en.wikipedia.org/wiki/OpenMP>.
- 11 *OpenMP Specifications*, <http://www.openmp.org/>.
- 12 **Rakić PS, Milašinović DD, Živanov Ž, Suvajdžin Z, Nikolić M, Hajduković M**, *MPI-CUDA parallelization of a finite-strip program for Geometric Nonlinear analysis: A hybrid approach*, *Advances in Engineering Software*, **42**(5), (2011), 273–285, DOI 10.1016/j.advengsoft.2010.10.008.
- 13 **Woodsend K, Gondzio J**, *Hybrid MPI/OpenMP Parallel Linear Support Vector Machine Training*, *The Journal of Machine Learning Research*, **10**, (2009), 1937–1953.